Gradient-Free Tracking of Unsteady Environmental Level Sets in Dynamic Environments by a Nonholonomic Robot [⋆]

Alexey Matveev [*,**] **Alexander Kapitonov** [**] **Ivan Berman** [**]
Valerii Chernov [**]

[*] *Department of Mathematics and Mechanics, Saint Petersburg University, St. Petersburg, Russia (e-mail: almat1712@yahoo.com).*
[**] *Faculty of Control Systems and Robotics, ITMO University, St. Petersburg, Russia (e-mail: kapitonov.aleksandr@itmo.ru, iaberman@itmo.ru, vachernov@itmo.ru).*

Abstract: A non-holonomic under-actuated planar robot is propelled via interaction of its actuators with a dynamic surrounding medium; a control input is the angular velocity of robot's self-rotation relative to the medium. Meanwhile, the motion of the medium is unknown and unpredictable; the relative surge speed is time-varying and treated as uncertain. There is an unpredictably varying scalar environmental field. From a remote initial location, the robot should reach the isoline where the field assumes a pre-specified value, and then should repeatedly run its length. Robot measures only the field value at the current location and has no access to the field gradient or parameters of the medium motion. To solve this task, at first conditions are established that are necessary for the mission to be feasible with the given limitations on the robot's dynamics. Then a navigation law is presented that solves the mission under slight and partly unavoidable enhancement of these conditions. This law is computationally inexpensive and directly converts the current sensory data into the current control in a reflex-like fashion. The performance of the law is rigorously justified by a global convergence result and is confirmed via computer simulation tests.

Keywords: Tracking environmental boundaries, Sensor-based navigation, Sliding-mode control

1. INTRODUCTION

The need in effective tools for localization and exploration of environmental boundaries has motivated an active research on using robotic platforms in such missions; see e.g., (Joshi et al., 2009; Krzyszton and Niewiadomska-Szynkiewicz, 2016; Wang et al., 2018; Kitts et al., 2018; Garuglieri et al., 2019). Applications include localization of oil slicks, polluted areas, and other spatially distributed natural phenomena whose boundary can be defined as the level set (isoline) where an environmental field, like concentration of a pollutant, assumes a certain critical value. A typical mission is to arrive at the isoline and then to repeatedly run its length, thus displaying the boundary. Such missions are often difficult due to the paucity of both a priori and sensory data about the field. In particular, neither the azimuth nor distance data on the isoline may be available insofar as sensors measure only the field value via an immediate contact with the measured entity.

In such a situation, static sensor networks may be expensive in various respects since a high density of deployment over a vast area and heavy communication and computational loads may be needed to achieve a suitable quality of observation (Udagepola, 2018). Mobile sensors offer more efficiency since they can autonomously provide a high deployment density only at the right place and even find its geometric location if the "right place" is initially defined by other means. To implement this potential, a navigation algorithm is required that allows mobile sensors to localize, approach, and cover the isoline of interest.

Much attention has been given to design of such algorithms. Many of them assume access to the field gradient (Hsieh et al., 2007; Srinivasan et al., 2008; Zhang and Leonard, 2010; Kitts et al., 2018); samples include off-springs of the 'snake' algorithms in image segmentation (Kitts et al., 2018), networked estimation of the field gradient (Zhang and Leonard, 2010), gradient-based contour estimation (Srinivasan et al., 2008; Kitts et al., 2018) and artificial potentials (Hsieh et al., 2007). However, direct measurement of the field gradient is a rare occurrence, and gradient estimation from noisy access to the field value is still an intricate issue. Also, such estimation classically assumes access to the field values in several close locations scattered to all dimensions, whereas the focus on the isoline requires concentration of sensors near this 1D curve. Finally, communication constraints may severely impede transmission of field measurements to a gradient estimator, wherever it might be built. Then every mobile sensor has to act individually for extended periods of distance and time.

The alternative, "gradient-free" methods do not attempt to evaluate the gradient and are well-fitted to scenarios with a single mobile sensor measuring the field value only. Switches among several steering angles, which are triggered with crossing pre-specified field values, are advocated in (Zhipu and Bertozzi, 2007; Joshi et al., 2009). This method gives rise to oscillations around a worthwhile trajectory, along with concerns on a waste of resources in course of systematic and mutually nullifying shifts sideways. Whereas these findings are not backed by rigorous and complete justification, (Baronov and Baillieul, 2007) not only offer a PD controller for driving a Dubins' car-like robot with an infinite control range along an isoline but also prove local stability for radial harmonic fields. Sliding mode (SM) controllers are offered for a Dubins' car-like robot with a finite control range, and their global convergence is rigorously justified for generic smooth steady (Matveev et al., 2012) and time-varying (Matveev et al., 2015a) fields. The findings of (Matveev et al., 2012) are extended on the case of multiple robots and a steady field in (Ovchinnikov et al., 2015).

Environmental threats and resource shortages are among reasons by which tracking environmental boundaries is becoming increasingly common. This sets forth special requirements, partly economic in nature, to involved mass-produced equipments: they should be cheap, relatively small-sized, energy and computationally efficient, easily switchable among various kinds of ecological data, and highly automated; consumption of the dynamic and energy resources is welcome to be close to the minimum essential level. However, the influence from the medium of operation, like a water or air flow, may be comparable with the control effort from the robot. In a common situation where the robot is propelled due to interaction of its actuators with the medium, this implies that the expected effect from the controller output can be drastically altered by the unpredictable environment. Hence control laws are needed that are not only resource saving but also robust against these uncertainties, and take into account the genesis of the actual control influence on the robot's body.

In the survey of literature on robotic navigation for tracking environmental boundaries, the authors failed to come across one addressing these issues. This paper is aimed at filling this gap, while overcoming intricacies and flaws related to gradient estimation and sideways fluctuations.

To this end, we study a planar non-holonomic and under-actuated robot of a Dubins aircraft or vessel type (Fossen, 2011; Lekkas et al., 2016), which travels in a dynamic medium. This model is classically used to describe, e.g., missiles, fixed wing aircrafts, torpedo-like UUV's, and marine surface vessels. The robot is driven by the angular velocity of rotation with respect to the medium, bounded in absolute value. Its relative surge speed is not under control, may be intricately prompted by various factors, and so is treated as uncertain; so are the extreme values of the relative angular velocity. The targeted environmental boundary is related to an unpredictably varying scalar field, which is arbitrary up to a few natural and partly unavoidable assumptions. The robot's sensing capacity is limited to pointwise measurement of the field value; the robot can also assess the rate at which this reading evolves over time via, e.g., numerical differentiation.

We start with disclosing conditions necessary for the mission to be feasible under the above limitations and uncertainties. Then we identify and justify a control paradigm that suffices to solve the mission under only slight and partly unavoidable enhancement of those conditions. This paradigm is embodied in a specific control law and backed by a mathematically rigorous global convergence result. This law is non-demanding with respect to both computation and motion. Theoretical results are confirmed by computer simulations based on real-world data.

The body of the paper is organized as follows. Section 2 offers the system description and the problem setup. Section 3 introduces the quantities characterizing the field and medium. The assumptions and necessary conditions are discussed in Sect. 4, Sect. 5 presents the navigation law and main theoretical results. In Sect. 6, this result is specified in a particular scenario. Section 7 reports on computer simulations, Sect. 8 offers brief conclusions. Due to the paper length limitation, the proofs of the presented results will be given in its full version.

2. SYSTEM DESCRIPTION AND PROBLEM SETUP

A planar robot travels in a moving medium, like air or water, and is controlled by the angular velocity u relative to the medium. Measures are taken to maintain a constant value of the relative surge speed v. However, they may succeed only partly and v may vary with time, although without approaching zero or reversing. The effect of the robot on the medium is assumed to be ignorable so that the robot's overall motion can be viewed as the superposition of the motions of the medium and the robot within.

There is an unpredictably varying scalar field $D(t, \boldsymbol{r}) \in \mathbb{R}$, where t is time and $\boldsymbol{r} \in \mathbb{R}^2$ is spatial location. The robot should locate and monitor the boundary $I_t(d_0) := \{\boldsymbol{r} : D(t, \boldsymbol{r}) = d_0\}$ of the polluted area $\{\boldsymbol{r} : D(t, \boldsymbol{r}) \geq d_0\}$ where the field exceeds a certain "dangerous" level d_0. In other words, it should reach the curve $I_t(d_0)$ and then repeatedly run its length. Since changes in D can be caused not only by the motion of robot's habitat medium (like, e.g., when an AUV explores an oil spill on the sea surface), the field and medium are viewed as independent entities.

Only the field value $d(t) := D[t, \boldsymbol{r}(t)]$ at the current location $\boldsymbol{r}(t)$ is accessible to the robot. It also assesses the rate $\dot{d}(t)$ at which this reading evolves over time via, e.g., numerical differentiation, although any method is welcome.

We put $\boldsymbol{e}(\theta) := [\cos \theta, \sin \theta]^\top$ and adopt the assumptions that warrant the classic Dubins aircraft or vessel model in a moving medium (Fossen, 2011; Lekkas et al., 2016):

$$\dot{\boldsymbol{r}} = v(t)\boldsymbol{e}(\theta) + \boldsymbol{V}(\boldsymbol{r}, t), \quad \dot{\theta} = u, \quad -\underline{u}(t) \leq u \leq \overline{u}(t). \quad (1)$$

Here $\boldsymbol{V}(\boldsymbol{r}, t)$ is the velocity of the medium particle $\boldsymbol{r}$ at time t and $v(t)\boldsymbol{e}(\theta)$ is robot's velocity with respect to the medium. The relative angular speed u is the control input.

It is required to design a controller that ensures the convergence $D[t, \boldsymbol{r}(t)] \to d_0$ (as $t \to \infty$) to the isoline. Its coverage is to be ensured thanks to the assumed robot's superiority in speed over the medium.

The relative surge speed v may change with time depending on various factors. Since their modeling and parameter

identification is typically a highly intricate matter, we do not come into respective details and handle $v(t)$ as the resultant factual speed, disregard details of its genesis, but assume that measures are taken by which the speed v and its rate of change are always kept within known bounds:

$$0 < \underline{v} \leq v(t) \leq \overline{v}, \qquad |\dot{v}(t)| \leq \overline{a} \quad \forall t. \qquad (2)$$

Likewise, $\underline{u}(t)$ and $\overline{u}(t)$ are extreme turning rates, which can be implemented in a known way, but depend on various factors and are in fact uncertain. Despite this, the robot is always able to turn in both directions:

$$\underline{u}(t), \overline{u}(t) \geq \underline{u} > 0 \qquad \forall t. \qquad (3)$$

Accordingly, the controller must attain the control objective $D[t, \boldsymbol{r}(t)] \to d_0$ for any speed profiles that meet (2) and (3). If this requirement is satisfied, the controller is said to *robustly track the isoline* $I_t(d_0)$.

3. PARAMETERS OF THE MEDIUM AND FIELD

We use the following concepts, notations, and conventions:

Positive angles are counted counterclockwise;
$Z_{\text{op}} = \{(t, \boldsymbol{r})\}$, operational zone of the robot;
$\langle \cdot; \cdot \rangle, \| \cdot \|$, standard inner product and norm in the plane;
$I_{t,\boldsymbol{r}} := I_t(\eta_{t,\boldsymbol{r}})$ (where $\eta_{t,\boldsymbol{r}} := D(t, \boldsymbol{r})$), dynamic spatial isoline that passes through the point $\boldsymbol{r}$ at time t;
$\varkappa(t, \boldsymbol{r})$, its signed curvature at this point and time;
$\lambda(t, \boldsymbol{r})$, its front speed at this point and time;
$\alpha(t, \boldsymbol{r})$, its front acceleration at this point and time;
$\omega(t, \boldsymbol{r})$, angular velocity of its rotation;
$[\boldsymbol{\tau}(t, \boldsymbol{r}), \boldsymbol{n}(t, \boldsymbol{r})]$, right-handed Frenet-Serret frame of $I_{t,\boldsymbol{r}}$;
$W_n(t, \boldsymbol{r}) := \langle W; \boldsymbol{n}(t, \boldsymbol{r}) \rangle$, normal projection of vector W;
$W_\tau(t, \boldsymbol{r}) := \langle W; \boldsymbol{\tau}(t, \boldsymbol{r}) \rangle$, tangential projection of W;
$\boldsymbol{r}_+(\Delta t | t, \boldsymbol{r})$, point where the $\boldsymbol{n}$-axis of the Frenet-Serret frame crosses the displaced isoline $I_{t+\Delta t}(\eta_{t,\boldsymbol{r}})$
$\boldsymbol{A}(t, \boldsymbol{r})$, acceleration of the medium particle $\boldsymbol{r}$ at time t;
$\Omega(t, \boldsymbol{r})$, spin (vorticity) of the medium;
$E(t, \boldsymbol{r})$, strain-rate tensor of the medium.

The zone Z_{op} will be detailed later on in (7). Formal definitions of $\varkappa, \lambda, \alpha, \omega$ are available in (Matveev et al., 2015b). The Frenet-Serrat frame is oriented so that the domain of greater field values is to the left when moving in the direction of $\boldsymbol{\tau}$. As is shown in (Matveev et al., 2015b), $\varkappa, \lambda, \alpha, \omega, \boldsymbol{\tau}, \boldsymbol{n}$ are well defined under the following.

Assumption 3.1. In an open vicinity $\mathcal{V}_{\text{op}}$ of Z_{op}, the field D is of class C^2, its 1st and 2nd derivatives are bounded, and the spatial gradient is separated from zero: $\wp := \|\nabla D\| \geq b_\nabla^{-1}$ in $\mathcal{V}_{\text{op}}$ for some constant $b_\nabla > 0$.

Here $\wp(t, \boldsymbol{r})$ characterizes the density of the isolines, i.e., their "number" within the unit distance from $I_{t,\boldsymbol{r}}$, where the "number" is evaluated by the range of field values observed on them; see (Matveev et al., 2015b) for details.

The medium velocity $\boldsymbol{V}$ is assumed to be of class C^1. The acceleration of a medium particle is the material derivative of this velocity: $\boldsymbol{A} = \boldsymbol{V}'_t + \boldsymbol{V}'_{\boldsymbol{r}} \boldsymbol{V}$. The symmetric strain-rate tensor $E = \frac{1}{2}[\boldsymbol{V}'_{\boldsymbol{r}} + (\boldsymbol{V}'_{\boldsymbol{r}})^\top]$; the vorticity is defined by means of $\frac{1}{2}[\boldsymbol{V}'_{\boldsymbol{r}} - (\boldsymbol{V}'_{\boldsymbol{r}})^\top] = \begin{bmatrix} 0 & -\Omega \\ \Omega & 0 \end{bmatrix}$ (Altenbach and Öchsner, 2018).

4. NECESSARY CONDITIONS AND ASSUMPTIONS

Proposition 1. Let the robot be able to track the isoline $I_t(d_0)$ in each of two directions, starting at any time t from any point on $I_t(d_0)$ and whenever (2) and (3) are met. Then at any t and for any $\boldsymbol{r} \in I_t(d_0)$,

$$\underline{v} \geq |\lambda[t, \boldsymbol{r}] - V_n[t, \boldsymbol{r}]|, \qquad (4)$$

$$|V_\tau[t, \boldsymbol{r}]| < \sqrt{\underline{v}^2 - (\lambda[t, \boldsymbol{r}] - V_n[t, \boldsymbol{r}])^2}, \qquad (5)$$

$$\underline{u} \geq \max_{v \in [\underline{v}, \overline{v}]} \left\{ \overline{a} |\lambda - V_n| / (v \mathfrak{v}_\tau) \right.$$
$$+ \left| \Omega + \langle E\boldsymbol{\tau}; \boldsymbol{n} \rangle \pm [A_n + \langle E\boldsymbol{n}; \boldsymbol{n} \rangle (\lambda - V_n)] / \mathfrak{v}_\tau \right.$$
$$\left. \mp [2(\pm \mathfrak{v}_\tau + V_\tau)\omega + \varkappa(\pm \mathfrak{v}_\tau + V_\tau)^2 + \alpha] / \mathfrak{v}_\tau \right| \right\}, \qquad (6)$$

where $\mathfrak{v}_\tau = \mathfrak{v}_\tau(v, t, \boldsymbol{r}) := \sqrt{v^2 - (\lambda - V_n)^2}$.

In (6), Ω is the angular velocity of rotation of an infinitesimally small volume of the medium, $\langle E\boldsymbol{\tau}; \boldsymbol{n} \rangle$ is the rate of its shear, i.e., the rate at which the angle between the axes of the Frenet-Serrat frame deviates from $\pi/2$ as they are transported by the medium, and $\langle E\boldsymbol{n}; \boldsymbol{n} \rangle$ is the rate at which an infinitesimally small segment normal to the isoline is stretched by the medium motion (Altenbach and Öchsner, 2018).

Thus (4)–(6) must hold on $I_t(d_0)$ for the control objective to be realistic. Also, controllability of the output d is classically claimed to regulate it to the targeted value d_0: from tracking an isoline $I_t(d_*)$, the robot should be able to turn so that the field increases, as well as so that it decreases. As can be shown, this capacity implies (4)–(6) on $I_t(d_*)$ and, conversely, is implied by (4)–(6) if $\leq$ is replaced by $<$ there. Such controllability is a matter of concern in Z_{op}. For the sake of convenience, we characterize Z_{op} in terms of the extreme values $d_- \leq d_+$ (such that $d_- \leq d_0 \leq d_+$) taken by the field in this zone:

$$Z_{\text{op}} := \{(t, \boldsymbol{r}) : d_- \leq D(t, \boldsymbol{r}) \leq d_+\}. \qquad (7)$$

As a result, we arrive at the following.

Assumption 4.1. There exist $\Delta_v \in (0, \underline{v})$ and $\Delta_u \in (0, \underline{u})$ such that (4)–(6) hold in the entire operational zone and even if $\underline{v} \mapsto \underline{v} - \Delta_v$ and $\underline{u} \mapsto \underline{u} - \Delta_u$.

The next assumption is typically met in the real world.

Assumption 4.2. In $\mathcal{V}_{\text{op}}$ from Asm. 3.1, the acceleration, spin, and rate of deformation of the medium are bounded

$$\|\boldsymbol{A}\| \leq \overline{A}, \quad \|\Omega\| \leq \overline{\Omega}, \quad \|E\| \leq \overline{E}. \qquad (8)$$

Let $\mathfrak{T}_\pm$ be the trajectory that emerges from the initial state $\boldsymbol{r}_{\text{in}}, \theta_{\text{in}}$ under the extreme actuation $\mathfrak{u} \equiv \underline{u}(t)/\mathfrak{u} \equiv \overline{u}(t)$.

Assumption 4.3. There exists time T such that as t runs from 0 to T, (a) each trajectory $\mathfrak{T}_\pm$ lies in Z_{op}, (b) on this trajectory, $\nabla D[t, \boldsymbol{r}(t)]$ rotates through an angle which does not exceed $\Delta_\theta - 2\pi$, where Δ_θ is the absolute value of the associated change in the angle θ from (1).

In other words, the field gradient rotates at a lesser average rate than the the robot's velocity relative to the medium.

Now we illustrate Asm. 4.3 by examples where it is met.

1. The medium, field, and robot are steady: $\boldsymbol{V} \equiv 0$, $D(t, \boldsymbol{r}) = D(\boldsymbol{r})$, $v(t) \equiv v$, $\overline{u}(t) \equiv \overline{u} \equiv -\underline{u}(t)$. Then Z_{op} is time-independent, and $\mathfrak{T}_\pm$ lies on the circle $C_\pm$ with a

radius of $R := v/\overline{u}$ that goes counterclockwise/clockwise through $\boldsymbol{r}_{\mathrm{in}}$ in direction of θ_{in}; the route over $C_\pm$ is completed for $T := 2\pi/\overline{u}$ time units. *Asm. 4.3 is met if the disk $D_\pm$ encircled by $C_\pm$ lies in Z_{op}.* Indeed, let t run from 0 to T. Then $\Delta_\theta = 2\pi$, and the robot eventually returns to the initial state. Since $C_\pm$ is homotopic in $D_\pm$ to the "staying still" $\boldsymbol{r}(t) \equiv \boldsymbol{r}_{\mathrm{in}}$ path and $\nabla D(\boldsymbol{r}) \neq 0 \forall \boldsymbol{r} \in D_\pm \subset Z_{\mathrm{op}}$ by Asm. 3.1, the angle of rotation of ∇D over these two paths is the same and so is equal to $0 \leq \Delta_\theta - 2\pi$.

2. Case 1, except for the field time-invariance. Then Asm. 4.3 *is fulfilled if there exists a natural k such that as t runs from 0 to $2\pi k/\overline{u}$, the disk $D_\pm$ lies in Z_{op} and $\nabla D[t, \boldsymbol{r}_{\mathrm{in}}]$ rotates through an angle $\leq 2\pi(k-1)$.* Indeed, now $\mathfrak{T}_\pm$ is composed of k full runs over $C_\pm$ and $\Delta_\theta = 2\pi k$. It remains to note that the angle of the gradient rotation over $\mathfrak{T}_\pm$ equals that of rotation over the "staying still" trajectory by the above homotopy-based argument.

5. NAVIGATION LAW AND MAIN RESULTS

We examine the following navigation law:

$$u(t) := \frac{1}{2}[(1-\sigma)\underline{u}(t) + (1+\sigma)\overline{u}(t)], \quad \text{where}$$

$$\sigma := -\mathbf{sgn}\{\dot{d}(t) + \mu\chi[d(t) - d_0]\}. \quad (9)$$

Here $\mathbf{sgn}\, a$ is the sign of a ($\mathbf{sgn}\, 0 := 0$), $\mu > 0$ is a parameter of the controller, and $\chi(\cdot) : \mathbb{R} \to \mathbb{R}$ is a designer-chosen continuous piece-wise smooth function such that

$$\chi(z) < 0\ \forall z < 0, \quad \chi(z) > 0\ \forall z > 0, \quad (10)$$

$$\overline{\chi} := \sup_{z \in \mathbb{R}} |\chi(z)| < \infty, \quad \overline{\chi}' := \sup_{z \in \mathbb{R}} |\chi'(z\pm)| < \infty. \quad (11)$$

Examples are given by $\chi(z) = a\chi_*(z/b)$, where $a, b > 0$ and $\chi_*(z) = \arctan(z), \tanh(z), \frac{z}{\sqrt{1+z^2}}$.

Remark 5.1. According to the comments on $\underline{u}, \overline{u}$ that follow (2), implementation of (9) comes to executing two simple rules: 1) if $\sigma = -1$, apply maximum steering to the left, 2) if $\sigma = 1$, apply maximum steering to the right.

For the discontinuous control law (9), the closed-loop solution is meant in Fillipov's sense (Filippov, 1988).

While omitting rather cumbersome details of controller tuning, the first theorem highlights its principal feature: the control law (9) is intrinsically capable of achieving the control objective under minimal and partly unavoidable assumptions introduced in the previous section.

Theorem 5.1. Let (10), (11) and Assumptions 3.1, 4.1—4.3 hold. Then the parameter μ can be chosen so that **i)** the robot driven by the control law (9) always remains in the operational zone (7) and robustly tracks the targeted isoline, as is defined at the end of Section 2.

Remark 5.2. The first claim in **i)** means that the behavior of the field and medium outside the operational zone (7) does not matter. So Thm. 5.1 remains true if the assumptions about the field and medium are violated outside (7) and even if the field is not defined there. The last is of interest for some theoretical fields like $c \ln \|r\|$.

Remark 5.3. For the controller (9), the isoline is run in the direction of $\boldsymbol{\tau}$. Thm. 5.1 remains true if the sign is reversed in (9) ($\sigma = +\mathbf{sgn}\{\ldots\}$); then the direction inverses.

To actualize the conclusion of Thm. 5.1, it suffices to pick μ small enough. This can be viewed as a guideline for experimentally tuning the controller. Now we specify how small μ should be via providing explicit bounds. They can be used as a basis for analytically tuning the controller.

5.1 Analytically Tuning the Control Law

A prerequisite for this is availability of upper bounds on some physical characteristics of the field and medium. Along with the already introduced characteristics, they are concerned with the following ones:
$\overset{\bullet}{\wp}(t, \boldsymbol{r}) := \lim_{\Delta t \to 0} \frac{\wp[t+\Delta t, \boldsymbol{r}_+(\Delta t | t, \boldsymbol{r})] - \wp(t, \boldsymbol{r})}{\wp(t, \boldsymbol{r})\Delta t}$, logarithmic growth rate of the isoline density $\wp$ over time;
$\wp'_{\tau/n}(t, \boldsymbol{r}) := \lim_{\Delta s \to 0} \frac{\wp(t, \boldsymbol{r} + \boldsymbol{\tau}/\boldsymbol{n}\Delta s) - \wp(t, \boldsymbol{r})}{\wp(t, \boldsymbol{r})\Delta s}$, similar rate under a tangential/normal displacement at time t.

By Asm. 3.1 and the formulas linking D with the concerned characteristics (see e.g., (Matveev et al., 2015b)), these quantities are bounded in $\mathcal{V}_{\mathrm{op}}$ from Asm. 3.1:

$$|\wp'_{\tau/n}| \leq \overline{\wp}'_{\tau/n}, |\overset{\bullet}{\wp}| \leq \overset{\bullet}{\wp}{}^+, |\varkappa| \leq \overline{\varkappa}, |\omega| \leq \overline{\omega}. \quad (12)$$

We also invoke b_∇ from Asm. 3.1, Δ_v, Δ_u from Asm. 4.1, $\overline{v}, \underline{v}, \overline{a}$ from (2), $\overline{E}, \overline{V}$ from (8), and $\overline{\chi}, \overline{\chi}'$ from (11). We also use upper bounds $\overline{\mathbf{sp}} < \underline{v}$ and $\overline{\mathbf{ac}}$ on the relative front speed $\lambda - V_n$ and acceleration $\alpha - A_n$ of the isoline, respectively. Thanks to the argument underlying (8), we, for example, may put $\overline{\mathbf{sp}} := \underline{v} - \Delta_v$ based on (4) and Asm. 4.1, and $\overline{\mathbf{ac}} := \overline{\alpha} + \overline{A}$, where $\overline{A}$ is taken from (8) and $\overline{\alpha}$ is an upper bound on the front acceleration of the isoline.

Theorem 5.2. Let (10), (11) and Asm. 3.1, 4.1—4.3 hold and μ in (9) is chosen so small that the following holds:

$$\mu_\dagger := \mu b_\nabla \overline{\chi} < \underline{v} - \overline{\mathbf{sp}}, \quad (13)$$

$$\Delta_u \mathfrak{v}_\tau^3 > \mu_\dagger(\overline{\mathbf{sp}} + \mu_\dagger)\Big\{ (\overline{a}/\underline{v} + \overline{E})\overline{\mathbf{sp}} + 2(\overline{v} + 2\underline{v})\overline{\omega}$$

$$+\overline{\varkappa}(\overline{v} + \underline{v})^2 + \overline{\mathbf{ac}} + 2\overline{\varkappa}(\overline{v} + \underline{v})\underline{v}$$

$$+\frac{\underline{v}^3}{\overline{\mathbf{sp}} + \mu_\dagger}\Big[\frac{\mu_\dagger\overline{\chi}'}{\overline{\chi}b_\nabla} + \mu_\dagger\overline{\wp}'_n + \overset{\bullet}{\wp}{}^+ + \overline{\wp}'_\tau(\overline{v} + \underline{v})\Big]\Big\}, \quad (14)$$

$$\text{where} \quad \mathfrak{v}_\tau := \sqrt{\underline{v}^2 - (\overline{\mathbf{sp}} + \mu_\dagger)^2} > 0. \quad (15)$$

Then the claim **i)** from Thm. 5.1 is true.

Both (13) and (14) are satisfied if μ is small enough since the r.h.s. of (14) goes to zero as $\mu \to 0$. Also, the conclusion of Thm. 5.2 holds whenever the concerned characteristics of the medium and field obey the bounds used in (13), (14). This means that the examined control law is robust against any uncertainties within these bounds.

6. PARTICULAR SCENARIO

Now we discuss specification of the above assumptions and recommendations (13), (14) in a more particular scenario than that delineated in Sects. 2 and 4. Within the great diversity of such scenarios, our current choice is largely motivated by the paper length limitation.

The field D is the concentration of a substance that is transported by the stream of an ideal incompressible fluid via pure convection with no diffusion. This context is captured by

$$\mathbf{div}\boldsymbol{V} = 0, \qquad D'_t + \langle \nabla D; \boldsymbol{V} \rangle = 0, \quad (16)$$

where the former and the latter reflect incompressibility and the above features of the field transport, respectively.

Proposition 2. Under the conditions (16), the criterion for the mission feasibility from Prop. 1 shapes into

$$|V_\tau| < \underline{v}, \qquad \underline{u} \geq \left| \Omega + \langle E\boldsymbol{\tau}; \boldsymbol{n} \rangle \right| + |\varkappa|\overline{v}. \qquad (17)$$

Asm. 4.1 requests its fulfilment in the entire Z_{op} and with time-and location-independent gaps $\Delta_v > 0$ and $\Delta_u > 0$:

$$\Delta_v < \underline{v} - |V_\tau|, \quad \Delta_u < \underline{u} - \left| \Omega + \langle E\boldsymbol{\tau}; \boldsymbol{n} \rangle \right| - |\varkappa|\overline{v}. \quad (18)$$

Also, the recommendations (13) and (14) (under which **i)** from Thm. 5.1 holds by Thm. 5.2) take the form

$$\mu_\dagger := \mu b_\nabla \overline{\chi} < \underline{v}, \qquad (19)$$

$$\Delta_u > \frac{\mu_\dagger}{(\underline{v}^2 - \mu_\dagger^2)^{3/2}} \Big\{ 2\mu_\dagger(\overline{v} + 3\underline{v})[\overline{\Omega} + \overline{E}] + \mu_\dagger \overline{\varkappa}(\overline{v} + 3\underline{v})^2$$

$$+ \underline{v}^3 \Big[\mu_\dagger \overline{\chi}'/(\overline{\chi} b_\nabla) + \mu_\dagger \overline{\wp}_n' + \overline{E} + \overline{\wp}_\tau'(\overline{v} + 2\underline{v}) \Big] \Big\}. \qquad (20)$$

Prop. 2 does not involve the normal component V_n of the medium velocity and allows for any V_n's. This is because the robot and isoline are carried by the common medium flow. So to remain on the isoline, the robot needs the zero normal speed relative to the medium, which is available for any value of V_n. However to be able to move in the both (absolute) directions over the isoline, the tangential speed of the robot should exceed that of the medium, which gives rise to the first inequality in (17).

In the second inequality, $|\varkappa|\overline{v}$ is the robot's absolute angular velocity needed to track the isoline with the maximal possible speed $\overline{v}$, and $\Omega + \langle E\boldsymbol{\tau}; \boldsymbol{n} \rangle$ is the uncontrolled portion of this velocity induced by the rotation Ω and deformation $\langle E\boldsymbol{\tau}; \boldsymbol{n} \rangle$ of the medium. Since the control u is the relative angular velocity, the second inequality means that the needed absolute velocity can be produced under any circumstances within the limits (1) and (3).

If $\mu^2 \ll \mu, \mu_\dagger \ll \underline{v}$, the condition (20) can be heuristically simplified via dropping minor addends into $\Delta_u > \mu_\dagger \underline{v}^{3/2}[\overline{E} + \overline{\wp}_\tau'(\overline{v} + 2\underline{v})]$.

In (19) and (20), the field is represented by $b_\nabla, \overline{\varkappa}, \overline{\wp}_{\tau/n}'$. These are partly set by the fluid motion but also depend on the initial field profile. So further specification of (19) and (20) needs more data about this profile and the fluid motion. Discussion of relevant details is omitted due to the paper page limit and will be presented in its full version.

7. SIMULATION TESTS ON REAL-WORLD DATA

The studied scenario is especially interesting in environmental monitoring of water resources in an automatic mode. Indeed, a small motor vessel equipped with sensors, satellite navigation and an automatic control system is potentially capable of performing automatic concentration measurements of dissolved substances and various chemical indicators (temperature, electrical conductivity, turbidity, etc.). Meanwhile, application of our isoline tracking method for control of a real and expensive unmanned surface vessel requires preliminary experimental examination. Now we report on some results in this direction.

Our study was concerned with a solar-powered two hulls unmanned surface vessel of the catamaran type. It has two thrusters (bollard pull: 5.25 kgf); battery pack: 300 $W \times h$; photovoltaic panels: 200 W max; a set of sensors: temperature, dissolved oxygen, pH level, ions presence, etc; GPS navigation and motion control system based on

Pixhawk and PX4 autopilot; max velocity: $0.5 - 0.8 \ m/s$; dimensions: $1200 \times 1200 \times 500 \ mm$; weight: up to 38 kg; max measurement depth in water: $1.5 - 2 \ m$.

As the first stage of experimental validation of the control method, we performed a series of simulation tests based on real-world environmental data on the state of rivers and water bodies. These data were obtained from a series of measurements at discrete points along programmed meander-shaped paths in the territories of Kuibyshev reservoir (Togliatti, Russia) and pond of Aviatorov park (Saint-Petersburg, Russia). Data from the GPS module and sensors were linked to each other and fused into a state map of water with the following indicators: pH level (dimensionless), temperature ($^\circ C$), dissolved oxygen (%), electrical conductivity ($\mu S/cm$). For simulation tests, the obtained discrete data were converted into continuous fields using the natural neighbor interpolation. Further we will consider the field based on pH level data (Fig. 1).
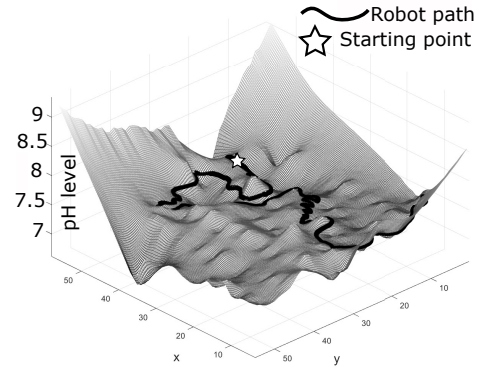

Fig. 1. pH field and example of its isoline tracking.

Simulations were carried out for the Dubins-car-like robot (1), the control law (9), and the following parameters: $v = 0.7 \ m/s$, $R_{min} = 0.5 \ m$, $\overline{u} = 1.4 \ rad/s$, $\mu = 8.3 \ 1/s$; the limited computing power of the on-board computer was modeled via delay $10^{-5} \ s$ in applying the control input. The controller parameters were chosen based on recommendations from Thm. 5.2. The extreme turning rate was calculated through the minimum turning radius ($\overline{u} = v/R_{min}$) because experiments with the real vessel have shown that the main limitation for the radius is at least half the vessel base width. Also, the measurements $d(t)$ were corrupted by additive band-limited white noise with power $A_n = 3 \cdot 10^{-11}$ and noise sample time $T_n = 3 \cdot 10^{-3}s$. The step time for all simulations is $2 \cdot 10^{-6} \ s$.

In the first test, data related to ponds, reservoirs and lakes were used (where the water is quite calm) and so the field was assumed static. Fig. 2(a) presents the results of simulation in static conditions without waves: bold straight line demonstrates robot path, dotted lines represent isolines with different levels. Fig. 2(b) demonstrates successful tracking of the desired field value $d_0 = 7.5$.

In the second test, the model was corrupted by sinusoidal waves $0.3 \cdot [\sin(0.05 \cdot x) + \sin(0.05 \cdot y)]$ and drift effect $0.008 \cdot t \cdot r_0$, where $r_0 = [\sin(0.087)\cos(0.087)]$. In accordance with (16), the model of wave formation in a water ensures its laminar movement. Moreover, the noise power were greatly increased: $A_n = 10^{-6}$, $T_n = 10^{-2} \ s$. Fig. 3 shows that the control objective is still achieved
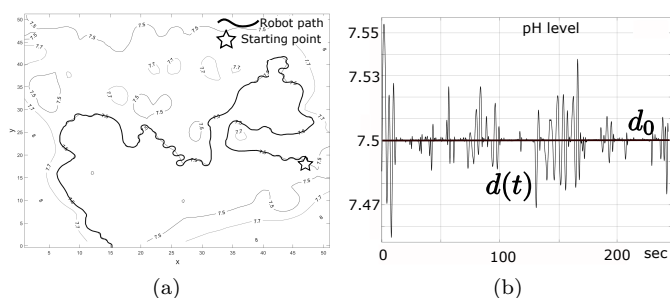
Fig. 2. Tracking of pH isoline (no waves, low noise).

with a good exactness: even a large noise, waves and drift causes rather satisfactory tracking accuracy.
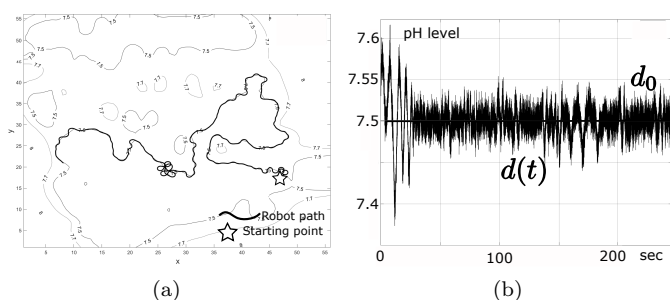

Fig. 3. Tracking of pH isoline (wave effects, high noise).

A comprehensive file containing the field maps, interactive Matlab plots (in .fig format) and multimedia (needs Matlab R2019a or higher) is available at `https://drive.google.com/open?id=1ujC_cyExpcoOlirFJLQTyAoMcTuKyQT8`.

8. CONCLUSIONS

The paper dealt with an under-actuated non-holonomic Dubins-vessel like robot that travels in the surge direction through a dynamic medium; the dynamics of the robot are essentially affected by this medium. The robot is controlled by the angular velocity of rotation with respect to the medium; the relative surge speed and extreme feasible angular velocities (in the clockwise and counterclockwise directions, respectively) are uncertain. The sensor data are limited to the field value at the vehicle current location. The paper presented a sliding-mode navigation law that drives the robot to the moving and deforming isoline of an unknown and time-varying scalar field and ensures its ultimate circulation along this curve. This law does not employ gradient estimation and is non-demanding with respect to both motion and computation. Its convergence was rigorously justified and its performance was confirmed by computer simulation tests based on real-wold data.

REFERENCES

Altenbach, H. and Öchsner, A. (eds.) (2018). *Encyclopedia of Continuum Mechanics*. Springer, Berlin.
Baronov, D. and Baillieul, J. (2007). Reactve exploration through following isolines in a potential field. In *Proc. of the American Control Conference*, 2141–2146. NY.
Filippov, A. (1988). *Differential Equations with Discontinuous Righthand Sides*. Kluwer Academic Publishers, Dordrecht, the Netherlands.

Fossen, T. (2011). *Handbook of Marine Craft Hydrodynamics and Motion Control*. Wiley, Chichester, UK.
Garuglieri, S., Madeo, D., Pozzebon, A., Zingone, R., Mocenni, C., and Bertoni, D. (2019). An integrated system for real-time water monitoring based on low cost unmanned surface vehicles. In *2019 IEEE Sensors App. Sym. (SAS)*, 1–6. IEEE.
Hsieh, M., Loizou, S., and Kumar, V. (2007). Stabilization of multiple robots on stable orbits via local sensing. In *Proc. of IEEE Conf. on Rob. and Autom.*, 2312 – 2317. Roma, Italy.
Joshi, A., Ashley, T., Huang, Y., and Bertozzi, A. (2009). Experimental validation of cooperative environmental boundary tracking with on-board sensors. In *Proc. of the ACC*, 2630 – 2635. St. Louis, MO.
Kitts, C.A., McDonald, R.T., and Neumann, M.A. (2018). Adaptive navigation control primitives for multirobot clusters: Extrema finding, contour following, ridge/trench following, and saddle point station keeping. *IEEE Access*, 6, 17625–17642.
Krzyszton, M. and Niewiadomska-Szynkiewicz, E. (2016). Heavy gas cloud boundary estimation and tracking using mobile sensors. *J. of Tel. and Inf. Tech.*, 3, 38–49.
Lekkas, A., Roald, A., and Breivik, M. (2016). Online path planning for surface vehicles exposed to unknown ocean currents using pseudospectral optimal control. *IFAC-PapersOnLine*, 49(23).
Matveev, A., Hoy, M., Ovchinnikov, K., Anisimov, A., and Savkin, A. (2015a). Robot navigation for monitoring unsteady environmental boundaries without field gradient estimation. *Automatica*, 62, 227–235.
Matveev, A., Hoy, M., and Savkin, A. (2015b). Proofs of the technical results justifying an algorithm of extremum seeking navigation in dynamic environmental fields. *arXiv*. Online: `http://arxiv.org/abs/1502.02224`.
Matveev, A., Teimoori, H., and Savkin, A. (2012). Method for tracking of environmental level sets by a unicycle-like vehicle. *Automatica*, 48(9), 2252–2261.
Ovchinnikov, K., Semakova, A., and Matveev, A. (2015). Cooperative surveillance of unknown environmental boundaries by multiple nonholonomic robots. *Robotics and Autonomous Systems*, 72, 164–180.
Srinivasan, S., Ramamritham, K., and Kulkarni, P. (2008). ACE in the hole: Adaptive contour estimation using collaborating mobile sensors. In *Proc. of the Int. Conf. on Inform. Processing in Sensor Networks*, 147 – 158. St. Louis, Missouri.
Udagepola, K. (2018). Mobile sensor networks and robotics. In *Internet of Things and Big Data Analytics Toward Next-Generation Intelligence*, 21–46. Springer.
Wang, Y., Engel, B.A., Huang, P., Peng, H., Zhang, X., Cheng, M., and Zhang, W. (2018). Accurately early warning to water quality pollutant risk by mobile model system with optimization technology. *J. of Env. Management*, 208, 122–133.
Zhang, F. and Leonard, N.E. (2010). Cooperative control and filtering for cooperative exploration. *IEEE Tran. on Automatic Control*, 55(3), 650–663.
Zhipu, J. and Bertozzi, A. (2007). Environmental boundary tracking and estimation using multiple autonomous vehicles. In *Proc. of the 46th IEEE Conf. on Decision and Control*, 4918–4923. New Orleans, Lu.